CrossMark
click for updates

View Article Online
View Journal

Journal of
Materials Chemistry A

Accepted Manuscript

This article can be cited before page numbers have been issued, to do this please use: A. Mahata, K. S. Rawat, I. Choudhuri and B. Pathak, *J. Mater. Chem. A*, 2016, DOI: 10.1039/C6TA03245A.

This is an *Accepted Manuscript*, which has been through the Royal Society of Chemistry peer review process and has been accepted for publication.

Accepted Manuscripts are published online shortly after acceptance, before technical editing, formatting and proof reading. Using this free service, authors can make their results available to the community, in citable form, before we publish the edited article. We will replace this *Accepted Manuscript* with the edited and formatted *Advance Article* as soon as it is available.

You can find more information about *Accepted Manuscripts* in the Information for Authors.

Please note that technical editing may introduce minor changes to the text and/or graphics, which may alter content. The journal's standard Terms & Conditions and the Ethical guidelines still apply. In no event shall the Royal Society of Chemistry be held responsible for any errors or omissions in this *Accepted Manuscript* or any consequences arising from the use of any information it contains.

ROYAL SOCIETY OF CHEMISTRY

www.rsc.org/materialsA

View Article Online
DOI: 10.1039/C6TA03245A

Single-layered Platinum Nanocage: A Highly Selective and Efficient Catalyst for Fuel Cell

Arup Mahata,[†] Kuber Singh Rawat,[†] Indrani Choudhuri,[†] Biswarup Pathak, [†,#,*]

[†]Discipline of Chemistry, School of Basic Sciences, Indian Institute of Technology (IIT) Indore, Indore, M.P., India
[#]Center for Material Science and Engineering, Indian Institute of Technology (IIT) Indore, Indore, M. P., India
Email: biswarup@iiti.ac.in

Published on 09 June 2016. Downloaded by University of Cambridge on 12/06/2016 09:27:53.

Journal of Materials Chemistry A Accepted Manuscript

Abstract

Developing a highly efficient catalyst for oxygen reduction reaction (ORR) is key to the performance of a fuel cell for future energy applications. ORR pathways are systematically studied on (111) facet of an octahedral single-layered platinum nanocage (Pt_{66}), enclosed by well-defined (111) facets. Energetic (cohesive energy), thermal (molecular dynamics simulation) and dynamic (phonon frequency) calculations are carried out to evaluate the stability of the nanocage. Thermodynamic (reaction free energies) and kinetic (free energy barriers, and temperature dependent reaction rates) parameters are investigated to find out the most pathway for ORR. The catalytic activity of the nanocage is investigated in greater detail toward their product selectivity (H_2O vs. H_2O_2). The previous theoretical and experimental reports on bulk Pt(111) show that direct O-O bond dissociation and OH formation is very much unlikely due to the high-energy barrier. However, we find that the direct O-O bond dissociation and OH formation is thermodynamically and kinetically favourable when catalysed by an octahedral Pt-nanocage. Our microkinetic analysis shows that the nanocage is a highly selective catalyst for the four-electron reduction ($*H_2O$ formation) over two-electron reduction ($*H_2O_2$ formation). The excellent catalytic activity of the nanocage is explained from the surface energy, compressive strain, Bader charge and density of states analysis.

Keywords: Heterogeneous Catalysis, Nanocage, Oxygen Reduction Reaction, Fuel Cell

View Article Online
DOI: 10.1039/C6TA03245A

Published on 09 June 2016. Downloaded by University of Cambridge on 12/06/2016 09:27:53.

Journal of Materials Chemistry A Accepted Manuscript

1. Introduction

Proton exchange membrane (PEM) fuel cell is one of the most promising devices for clean energy due to their high efficiency, low operating temperature and zero emission.[1-4] Oxygen reduction reaction (ORR) is the key reaction at the cathode and controls the performance of a fuel cell. However, Pt-based electrodes limit the performance of a fuel cell due to the sluggish ORR reaction rate and high overpotential.[5-6] As a result, the efficiency remains low, while the costs are very high for Pt-based electrodes. In the past few decades, considerable efforts (experimental and theoretical) have been made to improve the ORR activity. Pd and Ir based electrodes have been emerged as potential electrodes to sustain the harsh reaction conditions of the fuel cells.[7-10] However, due to their low abundances, the main challenge remains to lessen the cost of the catalyst. So, it is very important to design a highly active cheap electrode for ORR. However, the limited choice of such catalysts has made this a difficult task for the scientific community. Pt has been reported to be the most suitable catalyst among all for ORR. Thus, the key challenge is to reduce the Pt loading without compromising the performance of a fuel cell. In this context, alloying Pt with other transition metals has been emerged as a good alternative for efficiency and stability of the catalyst. Such alloying with other metals leads to the formation of bi-metallic,[11-13] mixed alloy[14-15] and core-shell structures.[16-18] These bi-metallic catalysts, not only reduce the Pt-content, but also increase the specific activity which in turns increase the efficiency of ORR activity. Norskov and co-workers[19-21] studied a series of Pt_3M alloy-based (M= Ti, V, Ni, Co, Fe, Y, Sc, Rh) catalysts for ORR activity and the low binding energy of the intermediate species (O and OH) on the alloy surfaces relative to Pt(111) bulk surface is the reason for their (Pt_3M, M = Co, Ni, Sc, Y) superior catalytic activities.

The discovery of fullerene[22] gave a new direction in the area of hollow materials. Later on, many fullerene like structures such as B-fullerene,[23] BN-fullerenes[24-25] and inorganic

View Article Online
DOI: 10.1039/C6TA03245A

Published on 09 June 2016. Downloaded by University of Cambridge on 12/06/2016 09:27:53.

fullerenes[26] have been synthesized for various applications. Similarly, metal-based hollow nanoclusters have been recently synthesized, which not only lower the Pt-content, but also improve the electro catalytic activity significantly. Recently, Pd-Rh nanoboxes[27] demonstrated excellent catalytic activity towards ORR. Xie and co-workers used an effective strategy for reducing the Pt-content by synthesizing atomic layer-by-layer deposition of Pt on Pd-nanocubes.[28] Besides, they have synthesized a series of octahedral-based nano-clusters,[29] by deposition of a few atomic layers (1-6 layers) of platinum on the Pd octahedral structure. Similarly, Pt-based cubic, octahedral[30] and icosahedral nanocages[31] have been synthesized with well defined (111) and (100) facets by depositing a few atomic layers of Pt on Pd nanocrystals and then etching away the Pd template. Considerable progresses have been made on the noble metal based nanocages, nanoframes and nanoboxes for ORR activity.[32-36] Recently, Adzic and co-workers synthesized a highly stable Pt monolayer on different substrate for ORR reactivity.[37-39] Interestingly, such nanocages show superior catalytic activity (towards ORR) compared to a Pt/C-based catalyst.[29-31] The developments in the field of single-layered materials inspired us to model a singled layered platinum-nanocage for ORR activity.

We report here for the first time that a single layered octahedral platinum nanocage (Pt_{66}) enclosed by eight (111) facets can improve the ORR activity significantly. Besides, the Pt-loading (lowers the Pt-content by 22%) of the nanocage for ORR is considerably lower than that of a similar size nanocluster (Pt_{85}).

Despite extensive experimental reports on ORR activity over a hollow nanocluster (such as nanocage, nanoframe, nanobox and so on), the underlying reason behind their excellent catalytic behaviour is yet to be understood. Thereby, the superior catalytic activity of the nanocage is investigated through a systemic study. The energetic, dynamic and thermal stability of this nanocage is verified by cohesive energy, phonon and molecular dynamics

Journal of Materials Chemistry A Accepted Manuscript

View Article Online
DOI: 10.1039/C6TA03245A

Published on 09 June 2016. Downloaded by University of Cambridge on 12/06/2016 09:27:53.

calculations, respectively. ORR involves many-electron reduction and it can proceed either through a more efficient four-step, four-electron reduction with the formation of H_2O or via a two-step, two-electron reduction for the formation of H_2O_2.[40] In fuel cells, four-electron reduction ($4e^-$) is preferred over a two-electron ($2e^-$) reduction in order to maximize the efficiency. Furthermore, H_2O_2 formation affects the durability of the membrane of a PEM fuel cell.[1,41] Thereby, the product selectivity [H_2O vs. H_2O_2] is very important for the performance of a Fuel Cell. The formations of *OH ($*O+H^++e^- \rightarrow *OH$) and $*H_2O$ ($*OH+H^++e^- \rightarrow *H_2O$) are the two most important steps for a platinum electrode-based fuel cell.[42-45] Therefore, the stability of the intermediate species (*O and *OH) is one of the governing factors for the selective four-electron ($4e^-$) reduction reaction. The adsorption behaviour of all the possible ORR intermediates and the complete O_2 reduction pathways are studied on Pt(111) facet of the nanocage surfaces. For comparisons, our results are compared with the available experimental and theoretical data on bulk Pt(111) surfaces. Microkinetic analysis is performed to gain more insights into the surface coverage, rate of reaction and product selectivity (H_2O vs. H_2O_2). The product selectivity (H_2O vs. H_2O_2) and exceptional catalytic activity of the nanocage are discussed at the end.

2. Model and Computational Details

An octahedral shape of ~1.5 nm diameter of Pt_{85} nanocluster is modelled by cutting along all (111) planes of the bulk face cantered cubic Pt structure. All the core atoms (19 atoms) of the Pt_{85} nanocluster are removed to create a void inside. Thus, the single layer nanocage (Figure 1a) structure consists of 66 platinum atoms. Pt-nanocages with icosahedral[31] and octahedral[30] geometries have been synthesized lately. Moreover, Pt(111) facet is the majorly exposed facet observed in the XRD pattern of experimentally synthesized Pt nanoclusters.[46-48]Previous

Journal of Materials Chemistry A Accepted Manuscript

View Article Online
DOI: 10.1039/C6TA03245A

Published on 09 June 2016. Downloaded by University of Cambridge on 12/06/2016 09:27:53.

experimental and theoretical reports show that Pt(111) surface shows better ORR activity than Pt(100) or any other Pt-surfaces[12,44,49-52]. Stamenkovic et al.[12] demonstrated through their experimental study that the Pt(111) surface shows two times higher ORR activity than the Pt(100) surface. Similarly, Zhang et al.[49] reported that Pt_3Ni nanoctahedra terminated with (111) facets improves the ORR activity by five-fold compared to the similar sized Pt_3Ni nanocube terminated with (100) facets. Carlos et al.[50] reported that the octahedral platinum nanoparticle with (111) facets exhibits an enhanced ORR activity while comparing with the cubic nanoparticles. Moreover, Markovic et al.[51] reported that the sequence of ORR activity on Pt(hkl) is (100) < (110) < (111).

Similarly, Duan et al.[44] reported from their theoretical study that Pt(111) surface shows better ORR activity compared to the Pt(100) surface. Moreover, Han et al.[52] stressed on the significant role of the square-symmetry of Pt(100) surface and reported that Pt(111) surface shows better catalytic activity compared to Pt(100) surface at the fuel cell operating voltage of around 0.7-0.8V. Therefore, inspired by these findings, we have designed an octahedral nanocage enclosed by (111) facets to improve the ORR activity.

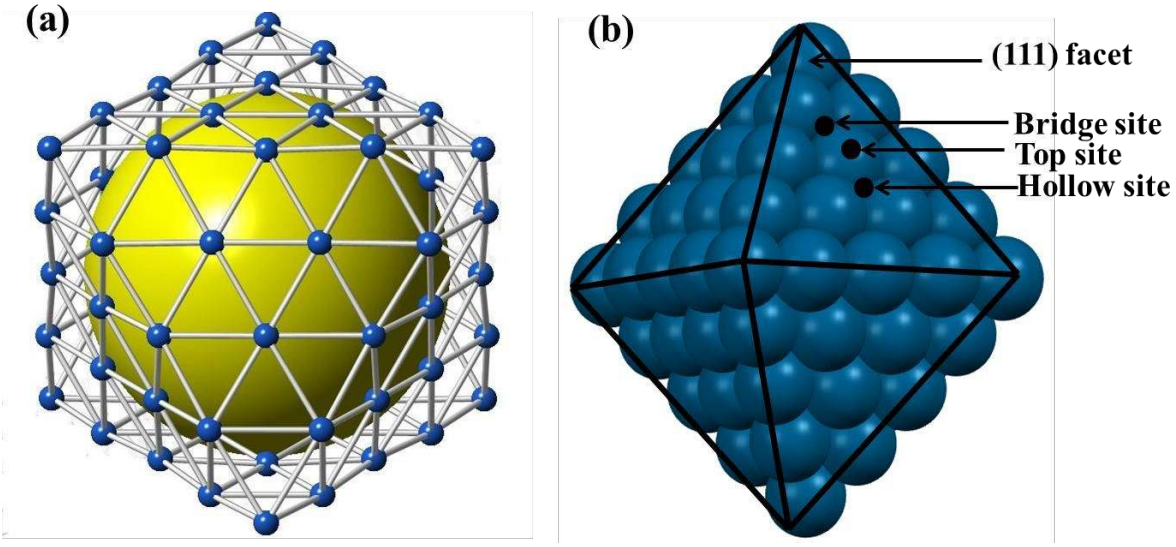

Figure 1: Octahedral nanocage with eight (111) facets: (a) yellow sphere represents the inside void of the nanocage and (b) different adsorption sites on (111) facet of the nanocage.

Journal of Materials Chemistry A Accepted Manuscript

View Article Online
DOI: 10.1039/C6TA03245A

Published on 09 June 2016. Downloaded by University of Cambridge on 12/06/2016 09:27:53.

The first-principles calculations are performed using a projected augmented wave (PAW)[53] method as implemented in the Vienna Ab initio Simulation Package (VASP).[54-56] The exchange-correlation potential is described by using the generalized gradient approximation of Perdew-Burke-Ernzerhof (GGA-PBE).[57] Projector augmented wave (PAW) method is employed to treat interactions between ion cores and valance electrons.[53] Plane wave with a kinetic energy cut off of 470 eV is used to expand the electronic wave functions. A 25 × 25 × 25 $Å^3$ cubic supercell is used to optimize the metal nanocage to rule out the possibility of interactions between the periodically repeated metal clusters. The nanocage is placed at the center of the box. During structural relaxation, all the atomic coordinates are optimized whereas the cell volume and cell shape are kept fixed. The Brillouin zone is sampled with a Gamma point (1×1×1) for clusters. The total energy of the nanocage cluster (Pt_{66}) is improved by 0.00003 eV if the k-point mesh set to 2 × 2 × 2. Therefore, we have used Gamma point for all the calculations to save the computational cost. All the atoms are relaxed for the full structural relaxation. The bulk Pt(111) surface is modelled with a (3 × 3) supercell to minimize the lateral interactions between the repeating images. The metal slab is composed of five atomic layers, where the bottom three layers are fixed and top two layers are relaxed. A 12 Å of vacuum is used along the z-direction to avoid periodic interactions. The Brillouin zone is sampled using a 3 × 3 × 1 k-point grid for the surface calculations. All the systems are fully optimized, where the convergence criteria for total energy and forces are set at 10^{-4} eV and <0.02 eV/Å, respectively. For electronic structure calculations, a 2 × 2 × 2 k-point mesh is used for the nanocage, whereas a 9 × 9 × 1 k-point mesh is used for bulk Pt(111) surface. Spin-polarized calculations are performed for all the molecular species and oxygen adsorbed intermediates. We have included Grimme's D3-type[58] of semiempirical method to include the dispersion energy corrections for van der Walls interactions. Phonon

Journal of Materials Chemistry A Accepted Manuscript

View Article Online
DOI: 10.1039/C6TA03245A

frequency of the nanocage is calculated using density functional perturbation theory.[59] The climbing nudged elastic band (CI-NEB) method[60] is used to locate the transition state. Six intermediate images are used in each CI-NEB pathway. Vibrational frequencies for the initial, transition and final states of the reactions are calculated and the transition states are confirmed by the presence of one imaginary frequency. Zero-point energy (ZPE) is calculated using the following equation:

$$ZPE = \sum_i 1/2h\upsilon_i$$

where h is the Planck constant and υ_i is the frequency of the i^{th} vibrational mode. The adsorption energies (E_{ad}) for all possible adsorbates are calculated using the following equation:

$$E_{ad} = E_{*\text{-adsorbate}} - (E_{*} + E_{adsorbate})$$

where $E_{*\text{-adsorbate}}$ is the total energies of the surface-adsorbate, E_{*} and $E_{adsorbate}$ are the single point energies of the surface and adsorbate in the optimized geometry of surface-adsorbate, respectively. We have used this convention for better comparisons, as the extent of deformation is different for different surfaces. The reaction free energy is calculated using the total energy difference between the products and the reactants. Thus, negative free energy suggests the exergonic nature of the reaction, whereas positive reaction energy suggests the endergonic nature of the reaction. Activation barriers are calculated by the energy differences between the transition and initial states. The reaction free energies(ΔG) and activation barriers ($\Delta G^{\ddagger}$) are calculated using zero point energy (ZPE) and entropy corrections. The adsorbed intermediate (R) is denoted with an asterisk (*) sign.

3. Results and Discussion

We have divided this section into three parts. In the first part, we have discussed about energetic, thermal and dynamical stability of the Pt-nanocage. Then, the adsorption behaviour

Published on 09 June 2016. Downloaded by University of Cambridge on 12/06/2016 09:27:53.

Journal of Materials Chemistry A Accepted Manuscript

View Article Online
DOI: 10.1039/C6TA03245A

of ORR intermediates on the nanocage surface is studied and compared with previous theoretical and experimental reports on Pt(111) bulk surfaces. Furthermore, all possible elementary steps are subsequently studied for ORR followed by an attempt is made to find out the underlying reason behind the excellent catalytic behaviour of the nanocage and its catalytic activity is compared with previously reported bulk Pt(111) surface based catalysts. Finally, the effect of applied voltage on the free energy diagram has been discussed and a detailed microkinetic analysis has been performed to explore the selectivity of four-electron vs. two-electron reduction reaction.

3.1. Nanocage Stability

Energetic Stability:

Total energy calculations are performed to evaluate the thermodynamic stability of the nanocage. Cohesive energy is calculated for the nanocage (Pt_{66}) to find out the possibility of synthesizing such a nanocage structure. For comparisons, we have calculated cohesive energies for bulk and Pt(111) surface. The calculated cohesive energies are -4.71, -5.47 and -5.71 eV/atom for the nanocage, bulk Pt(111) surface and bulk platinum, respectively. The cohesive energy indicates that the nanocage structure is less stable with respect to the bulk Pt(111). Our calculated cohesive energy value of bulk platinum is very much in agreement with the experimental value of -5.84 eV/atom.[61]

Thermal Stability

Low-temperature fuel cells (DMFC, PEMFC and AFC) are operated in the temperature range from 300 to 600 K.[5,16] Thus, the thermal stability of the nanocage is verified by carrying out Ab Initio Molecular Dynamics Simulations (AIMD) using canonical ensemble at 300-600 K with a time step of 1 femtosecond. Temperature control is achieved by nose thermostat

Published on 09 June 2016. Downloaded by University of Cambridge on 12/06/2016 09:27:53.

Journal of Materials Chemistry A Accepted Manuscript

View Article Online
DOI: 10.1039/C6TA03245A

model.[62] First, the structure is heated at 300 K with a time step of 1 femtosecond (fs) for 20 picoseconds (ps), but no structure reconstruction is found. The fluctuation of the total energy is smooth throughout the AIMD simulation (Figure 2a). Hence, the structure remains stable at room temperature. Furthermore, simulations using an NVT ensemble at 350, 400, 450, 550 and 600 K with a time step of 1 fs were carried for 20 ps. We have plotted the root mean square displacement (RMSD) as a function of time step (Figure 2b) for all the cases. Our RMSD plots show that atomic displacements are negligible at lower temperatures (300-450 K) but significant at higher temperatures (500-600 K). The snapshots of atomic configurations of Pt_{66}-nanocage at the end of MD simulations are shown in Supporting Information. We did not find any structural reconstruction (see Supporting Information) even after heating at 600 K for 20 ps. We have carefully investigated the structure of the nanocage during the AIMD simulation at higher temperatures (500-600 K). At 500 K, our RMSD vs. time step plot shows that RMSD value is significantly high around 2600 fs. We find that the diameter of the nanocage (14.69 Å) increases to 14.75 Å (see Fig. S4a, Supporting Information) at 2600 fs. Similarly the diameter of the nanocage increases to 14.97 Å (see Fig. S4b, Supporting Information) at 550 K. Interestingly at 600K, our plot shows that maximum atomic displacements occur in two stages. During the first maxima (around 5650- 7150 fs), the surface atoms are moving inwards and the cluster size reduces to 14.42 Å (see Fig. S4c, Supporting Information). In the second hump (9120-11880 fs), shows that the surface atoms are moving outwards and the average diameter of the nanocage increases to 15.04 Å (see Fig. S5e, Supporting Information). However, the structure returns back to the minimum energy structure at the end of the simulation. Thus, at higher temperatures, atomic displacements are maximum and at 600 K, atomic displacements are occurring in both ways (inwards and outwards). However, even at 600 K, inter-conversion is not possible to any other structures. Thereby, we predict that the nanocage can withstand temperatures as high as 600 K. These

Published on 09 June 2016. Downloaded by University of Cambridge on 12/06/2016 09:27:53.

Journal of Materials Chemistry A Accepted Manuscript

View Article Online
DOI: 10.1039/C6TA03245A

results demonstrate that the single layered nanocage is separated by high-energy barriers from other local minima structures.

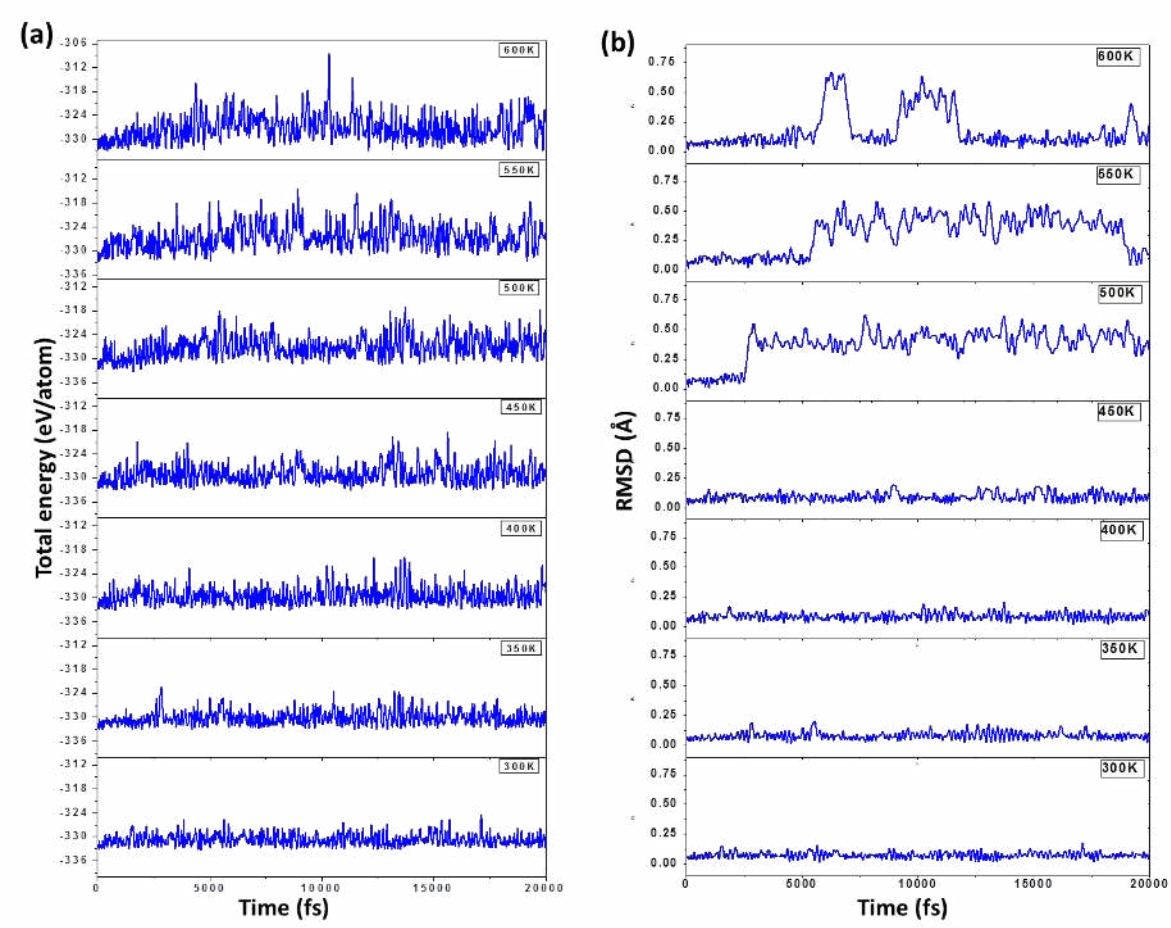

Figure 2: Molecular dynamics simulation analysis at different temperatures as a function of time step: (a) total energy and (b) RMSD.

Dynamic Stability:

The dynamic stability of the nanocage is evaluated from the phonon calculation by using Density Functional Perturbation Theory (DFPT) as implemented in VASP. Our phonon calculation on Pt_{66}-nanocage shows small imaginary frequencies in the order of <35i cm^{-1} (Supporting Information for details). Therefore, the nanocage could be a dynamically stable cluster. Generally, nanocages are synthesized on a support material[32] and in that case, they might show exceptional stability on a support material.

Published on 09 June 2016. Downloaded by University of Cambridge on 12/06/2016 09:27:53.

Journal of Materials Chemistry A Accepted Manuscript

View Article Online
DOI: 10.1039/C6TA03245A

Published on 09 June 2016. Downloaded by University of Cambridge on 12/06/2016 09:27:53.

Journal of Materials Chemistry A Accepted Manuscript

3.2 ORR Mechanism

3.2.1 Adsorption

Three different catalytic sites (Figure 1b) are present on Pt(111) facet of the nanocage: (i) top, (ii) bridge, and (iii) hollow. Here, fcc and hcp sites are equivalent and represented as a hollow site. We have checked the relative stabilities of the intermediate species (*O_2, *O, *OH, *OOH, *H_2O and *H_2O_2) adsorbed on all the three possible sites and then the most stable conformers are considered for detailed study. The most preferred binding sites of the intermediate species and their respective binding energies are calculated and given in Table 1. For comparison, we have calculated adsorption energy of the intermediate species on a bulk Pt(111) surface. Furthermore, all these values are compared (Table 1) with previous reported values on bulk Pt(111) surface to estimate the accuracy of our calculations.

Table 1: Preferred sites, binding energies (eV) of the most stable ORR intermediate species on Pt(111) facet of the nanocage and bulk Pt(111) surface. Here t, b, h and f denote top, bridge, hollow and fcc sites respectively. [63,64]Values are taken from the previous report on Pt(111) surfaces.

Adsorbed species	Nanocage (Pt_{66})	Pt(111) surface	Previous report of Pt(111) surface
*O_2	-1.82 (b)	-0.67 (b)	-0.69 (b)[63], -0.62 (b)[64]
*O	-5.32 (h)	-4.42 (f)	-3.96 (f)[63], -4.30 (f)[64]
*OH	-3.03 (b)	-2.37 (t)	-2.22 (t)[63], -2.21 (t)[64]
*OOH	-1.39 (b)	-1.15 (b)	-1.15 (b)[63], -0.94 (b)[64]
*H_2O_2	-0.22 (b)	-0.30 (b)	-0.37 (b)[63], -0.27 (b)[64]
*H_2O	-0.09 (t)	-0.26 (t)	-0.25 (t)[63], -0.20 (t)[64]
*H	-2.74 (h)	-2.77 (f)	-2.74 (f)[63], -2.62 (t)[64]

View Article Online
DOI: 10.1039/C6TA03245A

Published on 09 June 2016. Downloaded by University of Cambridge on 12/06/2016 09:27:53.

Journal of Materials Chemistry A Accepted Manuscript

***O_2**

*O_2 prefers to be adsorbed in a superoxo way on the bridge site of the nanocage with adsorption energy of -1.82 eV. However, the adsorption energy (for superoxo structure) is -0.67 eV while adsorbed on bulk Pt(111) surface. Thereby, O_2 is strongly adsorbed on the Pt_{66} nanocage surface compared to bulk Pt(111) surface. Furthermore, the adsorbed *O-O bond distances are 1.39, and 1.37 Å while adsorbed on nanocage and bulk Pt(111), respectively. Similarly, *O_2 can be adsorbed (via one of the O atoms) in a tilted way at the top site of Pt(111) facet of the nanocage with an adsorption energy -0.51 eV. The respective binding energy is -0.17 eV when adsorbed on bulk Pt(111) surface. This indicates that the nanocage is highly active for O_2 activation in relative to bulk Pt(111) surface.

Our calculated O_2 adsorption energy (-0.67 eV) while adsorbed in a superoxo fashion on bulk Pt(111) surface is very much in consistent with the previous calculated values of -0.41,[65] -0.49,[66] -0.62[64] and -0.69 eV[63] on bulk Pt(111) surface. The adsorption energy (-0.17 eV) calculated for the tilted conformer is also very much comparable with the previous calculated value of -0.06 eV.[66] In superoxo form, our calculated *O-O bond distance and vibrational frequency of O_2 bond while adsorbed on bulk Pt(111) surface are 1.37 Å and 879 cm^{-1}, which are also very much comparable with the experimental bond distance and vibrational frequency of 1.37 Å[67] and 870 cm^{-1},[68] respectively. The *O_2 superoxo form (-0.67 eV) is characterized experimentally through the temperature-programmed desorption technique and the experimentally reported binding energy of -0.38 eV[69] matches with our calculated binding energy of -0.67 eV. Using electron energy loss spectroscopy, Steininger *et al.*[70] reported the *O_2 binding energy of ≈ 0.5 eV, which is again very much in consistent with our calculated

View Article Online
DOI: 10.1039/C6TA03245A

adsorption energy of -0.67 eV. Thereby, we find that our results are in very much agreement with previously reported (theoretical and experimental) values.

***O**

*O is found to be more stable at the hollow site of the nanocage with adsorption energy of -5.32 eV. However, *O prefers fcc site of the bulk Pt(111) with a binding energy of -4.42 eV. Thereby, the nanocage is more reactive for *O binding. Previous surface model studies reported adsorption energies of -4.30,[64] -4.51 eV[71] and -4.46 eV[72] for *O binding at the fcc site of bulk Pt(111). Furthermore, our result is very much in agreement with experimental oxygen atom binding energy of 4.32 eV over a clean Pt(111) surface.[73]

***OH**

*OH prefers to be adsorbed at the bridge site of Pt(111) facet of the nanocage with an adsorption energy of -3.03 eV, which is higher than the adsorption energies (-2.37 eV) on bulk Pt(111) surface. Previous studies on bulk Pt(111) surfaces reported the adsorption energies of -2.21[64] and -2.45 eV[71] at the top position. Our calculated adsorption energy value on bulk Pt(111) is very much consistent with the experimental heat of formation of -2.14 eV over bulk Pt(111) surface.[74]

Interestingly, we find *O and *OH are strongly adsorbed over the nanocage surface compared to bulk Pt(111), which is far from optimal binding energy range of *O and *OH on Pt_3M alloy surfaces as proposed by Norskov and co-workers.[19-21]

***H_2O and *H_2O_2**

*H_2O adsorbs very weakly at the top site of (111) facet of the nanocage with an adsorption energy of -0.09 eV. In the bulk Pt(111) surface, *H_2O is calculated to be most stable at the top site with an adsorption energy of -0.26 eV, which is very much consistent with the

Published on 09 June 2016. Downloaded by University of Cambridge on 12/06/2016 09:27:53.

Journal of Materials Chemistry A Accepted Manuscript

View Article Online
DOI: 10.1039/C6TA03245A

previous theoretical adsorption energies of -0.20[64] and -0.22 eV.[65] The experimental binding energy of $*H_2O$ is -0.52 eV.[75] Gland *et al.*[76] reported the experimental adsorption energy of $*H_2O$ to be within 0.43-0.62 eV using the thermal desorption spectroscopy (TDS) and X-ray photoemmision spectroscopy (XPS). Our calculated adsorption energies of $*H_2O_2$ are -0.22 and -0.30 eV over the nanocage and bulk Pt(111), respectively. Previous theoretical studies reported the adsorption energies of -0.37[63] and -0.27 eV[64] over bulk Pt(111). The weak adsorption energy of $*H_2O$ and $*H_2O_2$ over the nanocage surface compared to Pt(111) suggests that the easy desorption of water from the catalyst surface. Therefore, reduces the possibility of surface poisoning.

Moreover, we have studied the adsorption behaviour of some important intermediates (O_2, O and OH) at the low-coordinated edge site to compare the catalytic activity of the edge site with respect to the Pt(111) surface of the nanocage. At the edge site, the calculated binding energies are -2.02, -4.72 and -3.02 eV for $*O_2$, *O and *OH, respectively. However, the respective binding energies are -1.82, -5.32 and -3.03 eV on the Pt(111) facet of the nanocage. We find that $*O_2$ adsorbs only in a superoxo way at the edge site of the nanocage with binding energy of -2.02 eV. However, at the edge site, we could not locate a minimum energy structure where $*O_2$ adsorbs in a titled way as observed on the Pt(111) surface. Thus, $*O_2$ has a higher binding energy (by 0.20 eV) at the edge site than on the Pt(111) facet of the nanocage. On the other hand, *O has a lower binding energy (by 0.60 eV), and *OH has a comparable binding energy at the edge site of the nanocage.

3.2.2 ORR Mechanism

During the ORR, H_2O and H_2O_2 are the two end products, which are formed via four-electron ($4e^-$) and two-electron ($2e^-$) reduction reactions, respectively. For the $4e^-$ reduction (H_2O

Published on 09 June 2016. Downloaded by University of Cambridge on 12/06/2016 09:27:53.

Journal of Materials Chemistry A Accepted Manuscript

View Article Online
DOI: 10.1039/C6TA03245A

formation), we propose two possible pathways: i) direct and ii) indirect (Scheme 1). In the direct pathway, the adsorbed oxygen molecule ($*O_2$) can undergo direct O-O bond dissociation ($*O_2 \rightarrow *O + *O$) and in the indirect mechanism, the reaction can precede via hydrogenation ($*O_2 + *H \rightarrow *OOH$) followed by dissociation ($*OOH \rightarrow *O + *OH$). Then the end products are formed through subsequent hydrogenation and O-H bond formation steps. However, the indirect bond dissociation can happen via two pathways: (i) peroxyl and (ii) peroxide formations. In the peroxyl mechanism, the adsorbed oxygen molecule ($*O_2$) undergoes hydrogenation ($*O_2 + *H \rightarrow *OOH$) followed by dissociation ($*OOH \rightarrow *O + *OH$). Then the product (*OH) can undergo subsequent hydrogenation for the formation of H_2O (major product). In the peroxide mechanism, *OOH can undergo further hydrogenation for the formation of $*H_2O_2$. This will be a two-electron reduction reaction if the end product is H_2O_2. However, $*H_2O_2$ can further dissociate into *OH, which can go for further protonation for the formation H_2O. Therefore, it is clear from the above three mechanisms that there are three important steps for four-electron ORR: (i) *O, (ii) *OH and (iii) $*H_2O$ formation steps.

The reaction free energies and activation barriers are calculated for all the possible elementary steps of ORR on the nanocage surface and then compared with previous reports on bulk Pt(111). Such comparison gives us an idea about the distinct nature of the nanocage-catalyst towards ORR activity.

Published on 09 June 2016. Downloaded by University of Cambridge on 12/06/2016 09:27:53.

Journal of Materials Chemistry A Accepted Manuscript

View Article Online
DOI: 10.1039/C6TA03245A

Published on 09 June 2016. Downloaded by University of Cambridge on 12/06/2016 09:27:53.

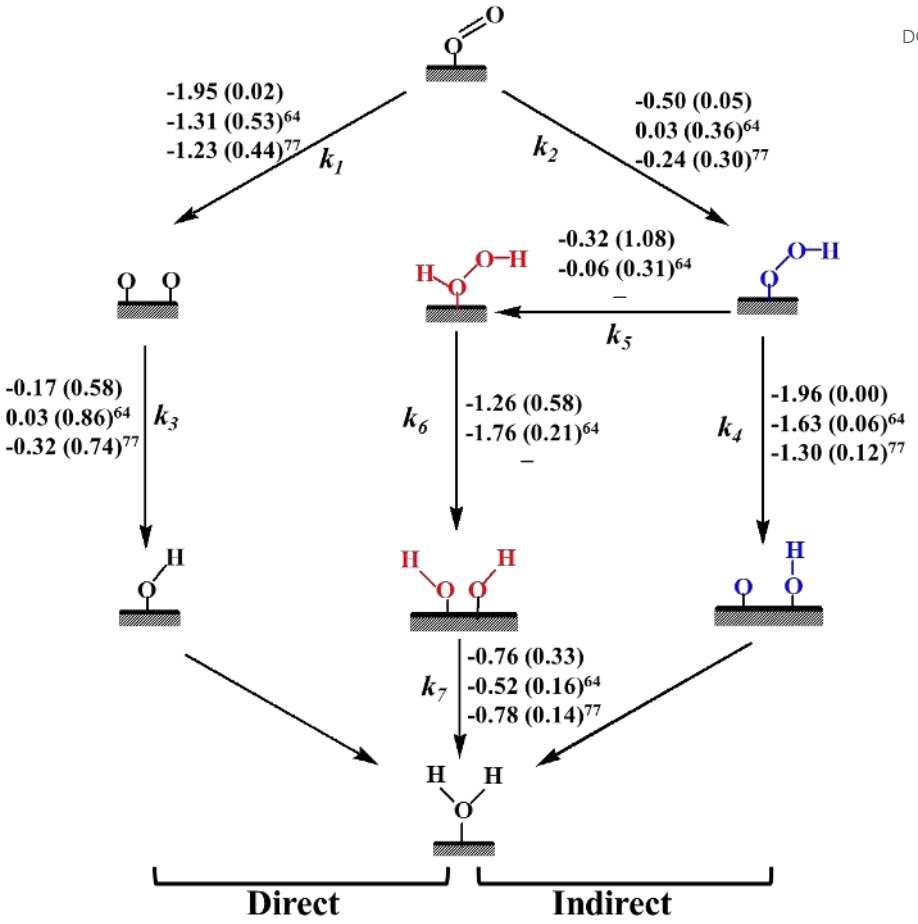

Scheme 1: Reaction free energies (eV) and activation barriers (eV, in parenthesis) are presented for all the possible elementary steps of ORR over (111) facet of the Pt_{66} nanocage. Our calculated respective values are compared with previous reports on oxygen reduction over Pt(111)[64,77] bulk surfaces.

O_2 activation:

Direct O-O bond dissociation is one of the very important steps for fuel cell application as it leads to the formation of H_2O, which reduces the formation of unwanted by-products. Thereby, direct dissociation favours $4e^-$ reduction over $2e^-$ reduction. Earlier studies show direct O-O bond dissociation (Step 1) is not kinetically favoured over O_2 hydrogenation (Step 2) on bulk Pt, Pd, Ag surfaces.[77-78] Thus, there are two competing pathways for $*O_2$ while

Journal of Materials Chemistry A Accepted Manuscript

View Article Online
DOI: 10.1039/C6TA03245A

adsorb on the catalyst surface. Either the adsorbed O_2 will dissociate into atomic oxygen *O or hydrogenated to *OOH.

$$*O_2 \rightarrow *O + *O \quad \Delta G = -1.95, \Delta G^{\ddagger} = 0.02 \text{ eV} \quad (1)$$

$$*O_2 + *H \rightarrow *OOH \quad \Delta G = -0.50, \Delta G^{\ddagger} = 0.05 \text{ eV} \quad (2)$$

As discussed, $*O_2$ can be adsorbed (see Supporting Information) via two conformers: (i) suproxo and (ii) titled.[66] The calculated O_2 dissociation (Step 1) barriers on the nanocage surface are 0.35 and 0.02 eV for superoxo and tilted conformers, respectively. Thus, during the activation process, the adsorbed $*O_2$ may rearrange itself from the superoxo to tilted conformer. In fact, the barrier (0.06 eV) is very low for such conformational rearrangement. Similar kind of observation reported on bulk Pt(111) surface.[66] The very low barrier for conformational rearrangement certainly favours the O_2 dissociation from the tilted conformer. The previously calculated O-O bond dissociation barriers are 0.53 eV[64] and 0.44 eV[77] on bulk Pt(111) and 0.72 eV and 1.22 eV on bulk Pd(111)[77] and Ag(111)[78] surfaces, respectively.

Similarly, O_2 hydrogenation (Step 2) on the nanocage surface is also exergonic (-0.50 eV) with an activation barrier of 0.05 eV. The barriers for the same step (Step 2) reported to be 0.25[63], 0.36[64] and 0.30 eV[77] on Pt(111) bulk surfaces. Therefore, the nanocage is highly reactive towards O_2 dissociation and favours direct O_2 bond dissociation over hydrogenation. This is opposite to other highly active catalysts such as Pt(111), Pd(111) and Ag(111), which favour hydrogenation over direct O_2 bond dissociation.

***OH formation**

The *OH formation is another important step for ORR and previous studies on bulk Pt(111) surfaces show[63-65,77] that this is one of the rate determining steps of ORR.

Published on 09 June 2016. Downloaded by University of Cambridge on 12/06/2016 09:27:53.

Journal of Materials Chemistry A Accepted Manuscript

View Article Online
DOI: 10.1039/C6TA03245A

Published on 09 June 2016. Downloaded by University of Cambridge on 12/06/2016 09:27:53.

Journal of Materials Chemistry A Accepted Manuscript

$$*O + *H \rightarrow *OH \qquad \Delta G = -0.17,\ \Delta G^{\ddagger} = 0.58 \text{ eV} \quad (3)$$

$$*OOH \rightarrow *O + *OH \quad \Delta G = -1.96,\ \Delta G^{\ddagger} = 0.00 \text{ eV} \quad (4)$$

The direct O-O bond dissociation followed by hydrogenation leads to the formation of *OH (Step 3). The direct formation of *OH (Step 3) on the nanocage surface is exergonic (-0.17 eV) with an activation barrier of 0.58 eV. Previous studies reported activation barriers of 0.74[77] and 0.86 eV[64] on bulk Pt(111) and 0.72 eV on Pd(111).[78]

Furthermore, *OH formation is possible via indirect pathways (Step 4) too; such as via peroxyl formation followed by O-O bond dissociation (Step 4). This step is a barrierless process on the nanocage surface with a reaction energy of -1.96 eV. Yao *et al.*[77] and Kai *et al.*[64] reported activation barriers of 0.12 eV and 0.06 eV for the *OOH dissociation (Step 4) step over bulk Pt(111) surfaces.

Though direct O-O bond dissociation (barrier 0.02 eV) is slightly favoured over O_2 hydrogenation (barrier 0.05 eV) but the OH formation (barrier 0.58 eV) is not favoured. On the other hand, indirect *OH formation (Step 4) is highly favourable on the nanocage surface. This suggests that *OOH will dissociate into *OH even if *OOH is formed on the nanocage surface. Thereby, the *OH formation is highly favoured via indirect pathway ($*O_2 + *H \rightarrow *OOH \rightarrow *OH$) than direct pathway ($*O_2 \rightarrow *O \rightarrow *OH$) on the nanocage surface.

Bader atomic charges[79] are calculated using Henkelman programme[80-82] to find out the net amount of charge transfer from the surface to intermediate species. Our Bader charge analysis shows that the charges on *O atoms are -0.70 |e| and -0.66 |e| while adsorbed on nanocage and bulk Pt(111) surfaces, respectively. The lower barrier for the *OH formation step (*O + *H → *OH) can be understood form the net negative charge gained at the O-atom from the surface Pt-atoms of the nanocage. We find that the adsorbed O-atom gains more negative

View Article Online
DOI: 10.1039/C6TA03245A

charge when adsorbed on the nanocage than on the bulk Pt(111) surface, owing to the strong adsorption of O-atom on the nanocage surface. The accumulation of more negative charge at the O-atom facilitates the protonation and thus the OH formation. As a result, the nanocage offers a different ORR pathways compared to the earlier reports.

Published on 09 June 2016. Downloaded by University of Cambridge on 12/06/2016 09:27:53.

***H_2O_2 formation and decomposition**

The two-electron reduction process leads to the formation of H_2O_2. H_2O_2 can be formed via two successive hydrogenations on O_2 ($*O_2 + *H \rightarrow *OOH$, $*OOH + *H \rightarrow *H_2O_2$).

$*OOH + *H \rightarrow *H_2O_2$ $\Delta G = -0.32$, $\Delta G^{\ddagger} = 1.08$ eV (5)

$*H_2O_2 \rightarrow *OH + *OH$ $\Delta G = -1.26$, $\Delta G^{\ddagger} = 0.58$ eV (6)

Thus, *OOH can undergo further hydrogenation for the formation of $*H_2O_2$ (Step 5). Our calculated activation barrier and free energy for this process are 1.08 and -0.32 eV respectively. Zhiyao *et al.*[63] reported activation barriers of 0.19 eV for H_2O_2 (Step 5) formation on bulk Pt(111) surface. This suggests that H_2O_2 formation is favoured on bulk Pt(111) surface. In contrary, the nanocage does not favour H_2O_2 formation. It indicates that the nanocage is highly selective for four-electron reduction over two-electron reduction. The $*H_2O_2$ can again dissociate into *OH (Step 6). The activation barrier for this step is 0.58 eV on the nanocage surface. Therefore, we predict that such nanocage could be a very selective catalyst for water formation and therefore could be a promising catalyst for fuel cell applications.

***H_2O formation**

$*OH + *H \rightarrow *H_2O$ $\Delta G = -0.76$, $\Delta G^{\ddagger} = 0.33$ eV (7)

Journal of Materials Chemistry A Accepted Manuscript

View Article Online
DOI: 10.1039/C6TA03245A

Published on 09 June 2016. Downloaded by University of Cambridge on 12/06/2016 09:27:53.

The adsorbed *OH undergoes protonation for the formation of $*H_2O$. On the nanocage surface, the activation barrier for this process is 0.33 eV with a reaction free energy of -0.76 eV. Previous studies reported H_2O formation barriers of 0.16 eV,[64] 0.09[63] and 0.14 eV[77] on bulk Pt(111) surfaces, which are lower than our calculated barrier of 0.33 eV on the nanocage surface. However, the $*H_2O$ formation barrier (0.33 eV) is lower than *OH formation (0.58 eV) barrier on the nanocage surface. This suggests that *OH formation is the rate determining step on the nanocage surface. It indicates that the $*H_2O$ formation will not influence the reaction kinetics on the nanocage surface. On the other hand, *OH formation barrier (0.58 eV) is significantly higher (0.74-0.86 eV) on bulk surface than the nanocage surface. Therefore, in spite of the high activation barrier for $*H_2O$ formation (Step 7), the nanocage catalyst is more efficient for ORR than any other catalysts reported so far. Moreover, $*H_2O$ adsorption energy is very low on the nanocage surface (-0.09 eV) compared to bulk Pt(111) surface (-0.26 eV), lessening the possibility of surface poisoning.

Therefore, our results show excellent catalytic activity of the nanocage toward ORR. This includes excellent catalytic activity toward rate-determining steps as well as for other important steps. We find that $*O_2$ activation processes ($*O_2 \rightarrow *O + *O$ and $*O_2 + *H \rightarrow *OOH$) and *OH formation ($*O + *H \rightarrow *OH$) are significantly improved over the nanocage surface.

In addition, we have also calculated the activation barriers for $*O_2$ dissociation ($*O_2 \rightarrow *O + *O$) and *OH formation ($*O + *H \rightarrow *OH$) steps at the low-coordinated edge site to compare the ORR activity at the edge site with respect to the Pt(111) surface of the nanocage. The activation barrier for the $*O_2$ dissociation is 0.21 eV at the edge site compared to 0.02 eV on the Pt(111) surface. This indicates $*O_2$ activation is easier on the surface than at the edge site. Similarly, the calculated activation barrier for the *OH formation is 0.77 eV at the edge site compared to 0.58 eV on the Pt(111) surface. Thereby, *OH formation is favourable on the

Journal of Materials Chemistry A Accepted Manuscript

View Article Online
DOI: 10.1039/C6TA03245A

Pt(111) surface than at the edge site. The high barriers for $*O_2$ dissociation and *OH formation could be due to the low adsorption energy of *O at the edge site.

It has been previously reported that compressive strain at the shell layer of core-shell structure could be the reason for enhancement of ORR performance.[83-84] Hence, the compressive/tensile strain energy (E_{strain}) is calculated using the following equation:

$E_{strain} = E_{unrelaxed} - E_{relaxed}$

where $E_{relaxed}$ is the total energy of the optimized cluster/surface and $E_{unrelaxed}$ is the total energy (single point energy) of the cluster in the bulk geometry. The strain (ε) is calculated using the following equation:

$\varepsilon = \Delta d/d$

where d is the diameter of the cluster/surface in its optimized structure and Δd is the change in the diameter from their bulk position.

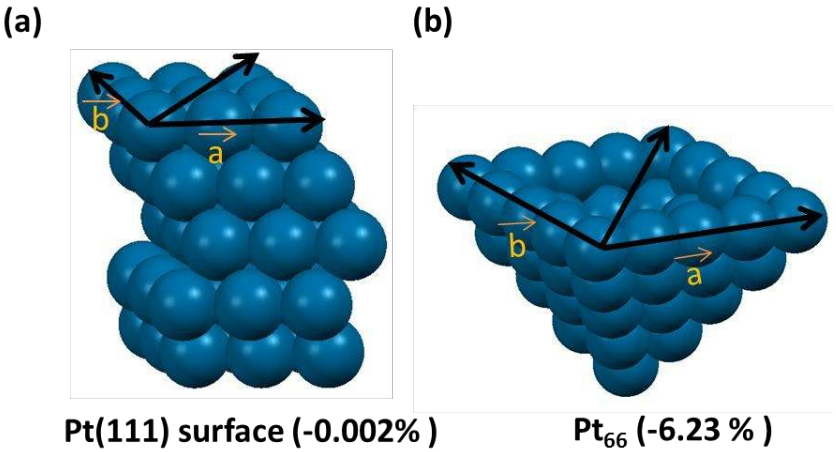

Figure 3: The compressive surface strain on (a) bulk Pt (111) and (b) nanocage.

The calculated (Figure 3) strain energies (compressive strain) for nanocage and bulk Pt(111) are 16.12(-6.23 %) and 0.32 eV(-0.002 %) respectively.

Published on 09 June 2016. Downloaded by University of Cambridge on 12/06/2016 09:27:53.

Journal of Materials Chemistry A Accepted Manuscript

View Article Online
DOI: 10.1039/C6TA03245A

Furthermore, we have calculated the surface energy of the nanocage to check its reactivity with respect to the bulk Pt(111) surface. The surface energy (E_{sur}) is calculated using the following equation:

$$E_{sur} = (E_{nanocage/surface} - E_{bulk})/ A_{nanocage/surface}$$

where, $E_{nanocage/surface}$ is the total energy of the nanocage/surface, E_{bulk} is the total energy of a bulk system containing the same number of atoms and $A_{nanocage/surface}$ is the total surface area of the nanocage/surface. The calculated surface energy for the Pt(111) surface and nanocage are 0.11 and 0.17 eV/atom respectively. The higher surface energy of the nanocage is reflected by the strong adsorption of the reaction intermediates also. Thus, Our adsorption, surface and strain energy analysis confirm that nanocage is highly reactive compared to the bulk Pt(111) surface.

The stronger adsorption of *O and *OH and weaker adsorption of $*H_2O$ can be further explained from their projected density of states (PDOS) analysis. Figure 4 shows that the Pt 3d orbitals of the nanocage are more stabilized while interacting with the O 2p orbitals of O/OH (Figure 4a-b). In contrary, the extent of stabilization (Figure 4a-b) is low while interacting with bulk Pt(111). The extent of orbital overlap is also high for *O and *OH adsorption, whereas low for $*H_2O$ adsorption (Figure 4c) on the nanocage surface.

Published on 09 June 2016. Downloaded by University of Cambridge on 12/06/2016 09:27:53.

Journal of Materials Chemistry A Accepted Manuscript

View Article Online
DOI: 10.1039/C6TA03245A

Published on 09 June 2016. Downloaded by University of Cambridge on 12/06/2016 09:27:53.

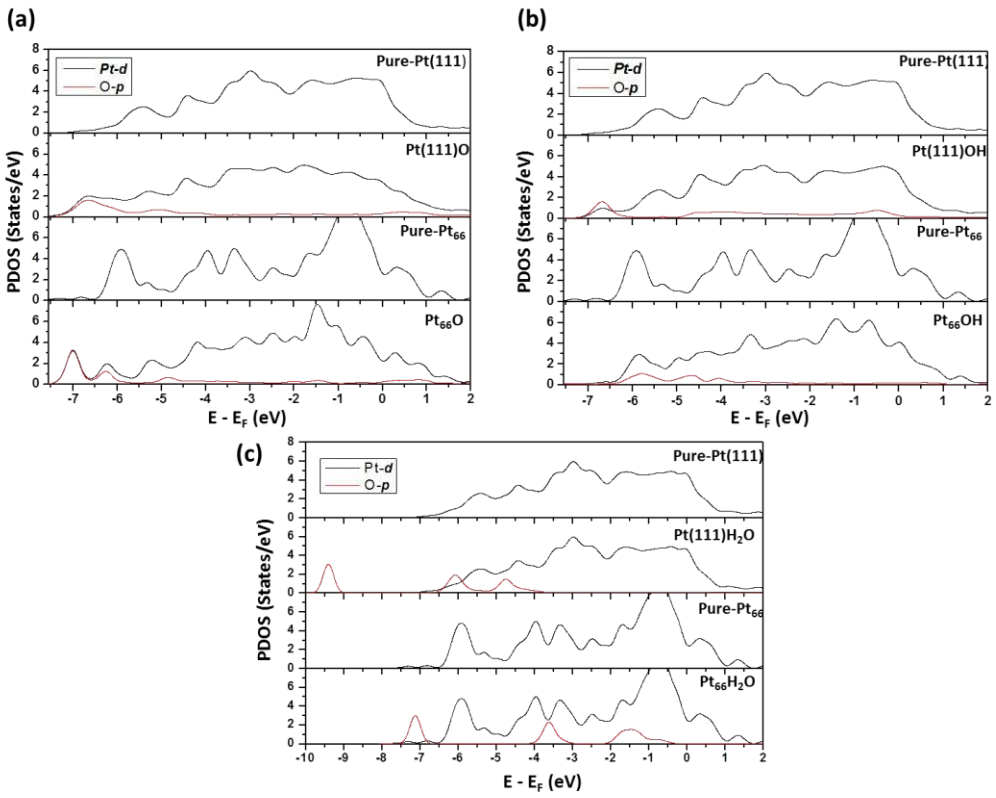

Figure 4: Projected density of states (PDOS) of (a) *O, (b) *OH and (c) *H_2O adsorbed Pt(111) and nanocage structures. PDOS of pure Pt(111) and nanocage (Pt_{66}) shown for comparison.

Therefore, our detailed investigation concludes that the void inside the nanocage induces a compressive strain in the system, which in turn improves the activity; thus the adsorption of the intermediates. The strong adsorption of the intermediates facilitates the charge transfer process (from the nanocage to adsorbed intermediates), which in turn improves the O-O dissociation and subsequent hydrogenation steps. As a result, it proceeds through a different mechanism (O-O dissociation followed by hydrogenation) than reported earlier (O-O hydrogenation followed by dissociation). This is in contrary to other bulk metal-based catalysts and therefore we believe that such nanocage-based catalysts can improve the ORR activity significantly.

Journal of Materials Chemistry A Accepted Manuscript

View Article Online
DOI: 10.1039/C6TA03245A

Published on 09 June 2016. Downloaded by University of Cambridge on 12/06/2016 09:27:53.

3.2.3 Effect of Applied Potential

Catalysts are exposed to electrical potential during the course of the reaction. Therefore, the effects of electrode potential on free energy and reduction mechanisms have been investigated as proposed by Norskov and co-workers.[42] The free energy change (ΔG) is calculated as follows:

$$\Delta G = \Delta E + \Delta ZPE - T\Delta S - eU$$

where ΔE is the total energy change obtained from the DFT calculations, ΔZPE is the change in zero-point energy, T is the room temperature (300 K), ΔS is the entropy change, e is the transferred charge for the elementary step and U is the electrode potential with respect to the standard hydrogen electrode.

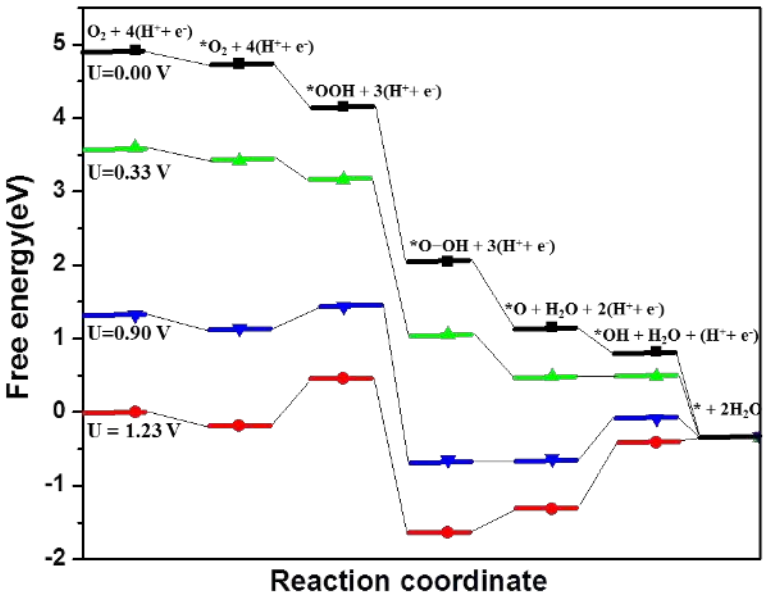

Figure 5: Free energy diagrams for ORR mechanism at different potentials

Journal of Materials Chemistry A Accepted Manuscript

View Article Online
DOI: 10.1039/C6TA03245A

Figure 5 shows that all the elementary steps are downhill process at U = 0 V. However, the proton transfer steps are thermodynamically not favourable as we increase the potential. Our calculated free energies show that the highest electrode potential under which all the elementary reactions are exergonic is 0.33 V. Thus, the working potential for the nanocage is 0.33 V and above this potential, some of the elementary reactions are endergonic. The *OH formation (*O + *H → *OH) step is not thermodynamically favourable at higher potentials. This suggests that the *OH formation is the rate determining step for ORR process, which is again very much in consistent with our kinetic study. However, *OOH and $*H_2O$ formations are less sensitive to applied potential. We have also studied the free energy diagram at 0.9 V (experimental operating potential) and we find that the $*H_2O$ formation is exergonic, whereas *OH formation is endergonic. It again indicates that *OH formation is the rate determining steps on the nanocage surface.

3.2.4 Kinetic Analysis

From the elementary pathways, we discover that many pathways are possible for O-O bond dissociation reaction. The reaction free energy versus reaction coordinate gives an overall idea to locate the minimum energy pathway from several possibilities. The roles of surface coverage, partial pressures (of reactant and product) and reaction temperature cannot be fully understood from the Gibbs free energy calculations. These experimental parameters can provide further insights into O_2 reduction reaction. Thus, we have done a detailed mickrokinetic analysis based on our preliminary DFT results to understand the roles of surface coverage, and reaction temperature toward the reaction kinetics. The forward (k_i) rate constants for all the elementary steps are calculated using the following equation:

$$k_i = \left(\frac{k_B T}{h}\right)\left(\frac{q_F}{q_I}\right) e^{-\Delta G^{\ddagger}/k_B T}$$

Published on 09 June 2016. Downloaded by University of Cambridge on 12/06/2016 09:27:53.

Journal of Materials Chemistry A Accepted Manuscript

View Article Online
DOI: 10.1039/C6TA03245A

where k_B is the Boltzmann constant, T is the temperature, h is the Plank constant. Here q_I and q_F are the vibrational partition functions for the initial and final state structures and $\Delta G^{\ddagger}$ is the Gibbs free energy barrier for the initial and final state of the elementary reaction. The vibrational partition functions (q) are calculated using the following equation:

$$q = \sum_i \frac{1}{1 - e^{-h\upsilon_i / k_B T}}$$

Where υ_i are the vibrational frequencies. All the exergonic reactions are assumed to be irreversible, hence only forward steps are considered for developing the microkinetic model. The details of the microkinetic model are given in the Supporting Information.

Table 2: Rate constants (s^{-1}) of the elementary reactions at different temperatures and here k_i stands for the forward step of i-th step.

Elementary reactions	300 K	350 K	400 K	450 K	500 K
$*O_2 \rightarrow *O + *O$ (k_1)	2.71×10^{12}	3.56×10^{12}	4.45×10^{12}	5.37×10^{12}	6.31×10^{12}
$*O_2 + *H \rightarrow *OOH$ (k_2)	1.11×10^{12}	1.68×10^{12}	2.34×10^{12}	3.06×10^{12}	3.84×10^{12}
$*O + *H \rightarrow *OH$ (k_3)	9.35×10^{02}	2.62×10^{04}	3.25×10^{05}	2.34×10^{06}	1.14×10^{07}
$*OOH \rightarrow *O + *OH$ (k_4)	3.64×10^{13}	3.37×10^{13}	3.24×10^{13}	3.19×10^{13}	3.19×10^{13}
$*H + *OOH \rightarrow *H_2O_2$ (k_5)	5.38×10^{-06}	2.43×10^{-03}	2.41×10^{-01}	8.77×10^{00}	1.57×10^{02}
$*H_2O_2 \rightarrow *OH + *OH$ (k_6)	1.08×10^{03}	3.15×10^{04}	4.04×10^{05}	2.30×10^{06}	1.18×10^{07}
$*H + *OH \rightarrow *H_2O$ (k_7)	2.29×10^{07}	1.62×10^{08}	7.15×10^{08}	2.30×10^{09}	5.93×10^{09}

As the oxygen reduction temperature in the low-temperature fuel cell ranges from 300 K to 500 K,[85-86] the rate constants (Table 2) are calculated in the same temperature range (300 K to 500 K). The rate constants improve significantly as we increase the temperature. At 300 K, the rate constants ratio between $*O_2$ dissociation and $*O_2$ hydrogenation (k_1/k_2) is 2.44. Hence, *O formation is highly favourable over *OOH formation ($*O_2 \rightarrow *O + *O$ and $*O_2 + *H \rightarrow *OOH$). Thus, we predict that the reaction might be proceeding through *OOH intermediate as the k_1/k_2 ratio is low. Therefore, it is important to examine the extent of possibility for proceeding the reaction further from the *OOH intermediate. The ratio of rate

Published on 09 June 2016. Downloaded by University of Cambridge on 12/06/2016 09:27:53.

Journal of Materials Chemistry A Accepted Manuscript

View Article Online
DOI: 10.1039/C6TA03245A

constants (k_4/k_5) for *OOH $\xrightarrow{k_4}$ *O + *OH and *OOH + *H $\xrightarrow{k_5}$ *H_2O_2 is 6.76×10^{18}, implying that the *OOH dissociation is favourable over *OOH hydrogenation. Therefore, even if the reaction proceeds through *OOH intermediate, it will dissociate into *O and *OH (*OOH → *O + *OH). Hence, our kinetic analysis suggests that the ORR favours four-electron reduction (H_2O formation) over two-electron reduction (H_2O_2 formation) on the nanocage surface.

The lesser possibility of two-electron reduction can be further confirmed from the microkinetic analysis. The ratio for the rate of formation of *H_2O and *H_2O_2 formations is 5.23×10^{44} under 1:1 partial pressure ratio of oxygen and hydrogen. Hence, the two-electron reduction is not favourable for the formation of hydrogen peroxide. This is very much in consistent with our activation barrier study, where we find that hydrogenation is favoured at *OH over *OOH. Therefore, the temperature dependant rate constant and mikrokinetic analysis show that single layered platinum nanocage is highly selective and efficient toward four-electron oxygen reduction reaction.

Conclusion

First-principles calculations are performed to understand the ORR activity on (111) facet of the octahedral nanocage (Pt_{66}) enclosed by well-defined facets. Energetic, thermal and dynamic stability of the nanocage evaluated from the total energy, AIMD simulation and phonon calculations, respectively. Molecular dynamics simulation suggests that the nanocage can withstand temperatures as high as 600 K without any structural reconstruction. During the ORR, H_2O and H_2O_2 are the two end products, which are formed via four-electron ($4e^-$) and two-electron ($2e^-$) reduction reactions, respectively. The reaction free energies and activation barriers are calculated for all the possible elementary steps of ORR on the

Published on 09 June 2016. Downloaded by University of Cambridge on 12/06/2016 09:27:53.

Journal of Materials Chemistry A Accepted Manuscript

View Article Online
DOI: 10.1039/C6TA03245A

nanocage surface and then compared with previous reports on bulk Pt(111). Our detailed investigation suggests that the nanocage induces a compressive strain in the system, which in turn improves the activity of the nanocage and thus improves the adsorption of the intermediates. Our results show that the *O and *OH adsorb strongly on the nanocage surface compared to bulk Pt(111) surface, which facilitates the charge transfer process (from the nanocage to adsorbed intermediates), which in turn improves the O-O dissociation and subsequent hydrogenation steps. As a result, the nanocage offers a different ORR pathways (O-O dissociation followed by hydrogenation) than the earlier reports (O-O hydrogenation followed by dissociation). This is completely opposite to the previous reports on Pt_3M (M = Ti, V, Ni, Co, Fe, Y, Sc, Rh) alloy based catalysts where the low binding energies of the reaction intermediates (*O and *OH) were credited for the superior catalytic activity. Our potential study indicates that the ORR is thermodynamically favourable at 0.33 V and *OH formation is the rate determining step. The rate determining step (*OH formation) is very much agreement with the kinetic study. Our microkinetic analysis shows that the H_2O formation is favoured over H_2O_2, which again suggests that the nanocage is highly selective for four-electron ORR over two-electron ORR. Hence, we report, platinum nanocage could be very promising catalysts for the efficient and selective reduction of O_2.

Supporting Information

Adsorption site of the most stable adsorbates, details of microkinetic analysis, snapshots of the nanocage after the simulation at different temperature, snapshots of the nanocage during the simulation at different temperatures and values of phonon frequencies have been given in Supporting Information.

Acknowledgments

Published on 09 June 2016. Downloaded by University of Cambridge on 12/06/2016 09:27:53.

Journal of Materials Chemistry A Accepted Manuscript

View Article Online
DOI: 10.1039/C6TA03245A

We thank IIT Indore for the lab and computing facilities. This work is financially supported by CSIR [Grant number: 01(2723)/13/EMR(II)] and DST-SERB.

Published on 09 June 2016. Downloaded by University of Cambridge on 12/06/2016 09:27:53.

Journal of Materials Chemistry A Accepted Manuscript

References

(1) Y. Jiao, Y. Zheng, M. Jaroniecb and S. Z. Qiao, *Chem. Soc. Rev.,* 2015, **44**, 2060.

(2) B. P. Vinayan, R. Nagar, N. Rajalakshmi and S. Ramaprabhu, *Adv. Funct. Mater.,* 2012, **22**, 3519.

(3) W. Lubitz and W. Tumas, *Chem. Rev.,* 2007, **107**, 3900.

(4) F. A. de Bruijn, V. A. T. Dam and G. J. M. Janssen, *Fuel Cells* 2008, **8**, 3.

(5) M. Watanabe, D. A. Tryk, M. Wakisaka, H. Yano, H. Uchida, *Electrochim. Acta* 2012, **84**, 187.

(6) F. Calle-Vallejo, M. T. M. Koper and A. S. Bandarenka, *Chem. Soc. Rev*. 2013, **42**, 5210.

(7) J. Wu and H. Yang, *Acc. Chem. Res.* 2013, **46**, 1848.

(8) E. Antolini, *ACS Catal.* 2014**, 4,** 1426.

(9)) O. Savadogo, K. Lee, K. Oishi, S. Mitsushima, N. Kamiya and K. I. Ota, *Electrochem. Commun.* 2004, **6**, 105.

(10) C. H. Wang, H. C. Hsu and K. C. Wang, *J. Colloid Interface Sci.* 2014, **427**, 91.

(11) Y. Xu, A. V. Ruban and M. Mavrikakis, *J. Am. Chem. Soc.* 2004, **126**, 4717.

(12) V. R. Stamenkovic, B. Fowler, B. S. Mun, G. Wang, P. N. Ross, C. A. Lucas and N. M. Marković, *Science* 2007, **315**, 493.

(13) V. Stamenkovic, B. S. Mun, K. J. J. Mayrhofer, P. N. Ross, N. M. Markovic, J. Rossmeisl, J. Greeley and J. K. Nørskov, *Angew. Chem.* 2006, **118**, 2963.

(14) W. J. Tang, L. Zhang and G. Henkelman, *J. Phys. Chem. Lett*. 2011, **2**, 1328.

(15) A. Holewinski, J. Idrobo and S. Linic, *Nat. Chem.*2014, **6**, 828.

View Article Online
DOI: 10.1039/C6TA03245A

(16) J. X. Wang, H. Inada, L. Wu, Y. Zhu, Y. Choi, P. Liu, W. P. Zhou and R. R. Adzic, *J. Am. Chem. Soc.* 2009, **131**, 17298.

(17) M. Oezaslan, F. Hasché and P. Strasser, *J. Phys. Chem. Lett.* 2013, **4**, 3273.

(18) V. Mazumder, M. Chi, K. L. More and S. Sun, *J. Am. Chem. Soc.* 2010, **132**, 7848.

(19) J. Greeley, I. E. L. Stephens, A. S. Bondarenko, T. PJohansson, H. A. Hansen, T. F. Jaramillo, J. Rossmeisl, I. Chorkendorff and J. K. Nørskov, *Nat. Chem.* 2009, **1**, 552.

(20) V. Stamenkovic, B. S. Mun, K. J. J. Mayrhofer, P. N. Ross, N. M. Markovic, J. Rossmeisl, J. Greeley, and J. K. Nørskov, *Angew. Chem. Int. Ed.* 2006, **45**, 2897.

(21) A. Jackson, V. Viswanathan, A. J. Forman, A. H. Larsen, J. K. Nørskov and T. F. Jaramillo, *ChemElectroChem* 2014, **1**, 67.

(22) H. W. Kroto, J. R. Heath, S. C. Obrien, R. F. Curl and R. E. Smalley, *Nature* 1985, **318**, 162.

(23) H. Zhai, Y. Zhao, W. Li, Q. Chen, H. Bai, H. Hu, Z. A. Piazza, W. Tian, H. Lu, Y. Wu, Y. Mu, G. Wei, Z. Liu, J. Li, S. Li and L. Wang, *Nat. Chem.* 2014, **6**, 727.

(24) X. Wang, Y. Xie and Q. Guo. *Chem. Commun.* 2003, 2688.

(25) A. Loiseau, F. Willaime, N. Demoncy, N. Schramchenko, G. Hug, C. Colliex and H. Pascard, *Carbon* 1998, **36**, 743.

(26) J. Bai, A. V. Virovets and M. Scheer. *Science*, 2003, **300**, 781.

(27) B. T. Sneed, C. N. Brodsky, C. Kuo, L. K. Lamontagne, Y. Jiang, Y. Wang, F. Tao, W. Huang and C. Tsung, *J. Am. Chem. Soc.* 2013, **135**, 14691.

(28) S. Xie, S. Choi, N. Lu, L. T. Roling, J. A. Herron, L. Zhang, J. Park, J. Wang, M. J. Kim, Z. Xie, M. Mavrikakis and Y. Xia, *Nano Lett.* 2014, **14**, 3570.

(29) J. Park, L. Zhang, S. Choi, L. T. Roling, N. Lu, J. A. Herron, S. Xie, J. Wang, M. J. Kim, M. Mavrikakis and Y. Xia, *ACS Nano* 2015, **9**, 2635.

Published on 09 June 2016. Downloaded by University of Cambridge on 12/06/2016 09:27:53.

Journal of Materials Chemistry A Accepted Manuscript

View Article Online
DOI: 10.1039/C6TA03245A

(30) L. Zhang, L. T. Roling, X. Wang, M. Vara, M. Chi, J. Liu, S. Choi, J. Park, J. A. Herron, Z. Xie, M. Mavrikakis and Y. Xia, *Science* 2015, **349**, 412.

(31) X. Wang, L. Figueroa-Cosme, X. Yang, M. Luo, J. Liu, Z. Xie and Y. Xia, *Nano Lett.* 2016, **16**, 1467.

(32) M. A. Mahmoud, D. O'Neil and M. A. El-Sayed, *Chem. Mater.* 2014, **26**, 44.

(33) Z. Fang, Y. Wang, C. Liu, S. Chen, W. Sang, C. Wang and J. Zeng, *Small* 2015, **11**, 2593.

(34) A. Popa and A. C. Samia, S. *Chem. Commun.* 2014, **50,** 7295.

(35) C. Chen, Y. Kang, Z. Huo, Z. Zhu, W. Huang, H. L. Xin, J. D. Snyder, D. Li, J. A. Herron, M. Mavrikakis, M. Chi, K. L. More, Y. Li, N. M. Markovic, A. Somorjai, G. P. Yang and V. R. Stamenkovic, *Science* 2014, **343**, 1939.

(36) X. Hong, D. Wang, S. Cai, H. Rong and Y. Li, *J. Am. Chem. Soc.* 2012, **134**, 18165.

(37) K. Sasaki, H. Naohara, Y. Choi, Y. Cai, W. Chen, P. Liu and R. R. Adzic, *Nat. Commun.* 2012, **3**, 1115.

(38) K. Sasaki, H. Naohara, Y. Cai, Y. M. Choi, P. Liu, M. B. Vukmirovic, J. X. Wang and R. R. Adzic, *Angew. Chem., Int. Ed.* 2010, **49**, 8602.

(39) J. Zhang, M. B. Vukmirovic, Y. Xu, M. Mavrikakis and R. R. Adzic, *Angew. Chem. Int. Ed.* 2005, **44,** 2132.

(40) E. Yeager, *J. Mol. Catal.* 1986, **38**, 5.

(41) C. M. Sanchez-Sanchez and A. J. Bard, *Anal. Chem.,* 2009, **81**, 8094.

(42) J. K. Nørskov, J. Rossmeisl, A. Logadottir, L. Lindqvist, J. R. Kitchin, T. Bligaard and H. Jonsson, *J. Phys. Chem. B* 2004, **108**, 17886.

(43) V. Tripkovic, E. Skulason, S. Siahrostami, J. K. Nørskov and J. Rossmeisl, *Electrochimica Acta*, 2010, **55**, 7975.

(44) Z. Duan and G. Wang, *J. Phys. Chem. C* 2013, **117**, 6284.

Published on 09 June 2016. Downloaded by University of Cambridge on 12/06/2016 09:27:53.

Journal of Materials Chemistry A Accepted Manuscript

View Article Online
DOI: 10.1039/C6TA03245A

(45) H. C. Tsai, Y. C. Hsieh, T. Yu, Y. J. Lee, Y. H.; Wu, B. V. Merinov, P. W. Wu, S. Y. Chen, R. R. Adzic and W. A. Goddard III, *ACS Catal.* 2015, **5**, 1568.

(46) T. Maiyalagan and F. N. Khan, *Catal. Commun.* 2009, **10**, 433.

(47) B. Zhang, D. Wang, Y. Hou, S. Yang, X. H. Yang, J. H. Zhong, J. Liu, H. F. Wang, P. Hu, H. J. Zhao and H. G. Yang, *Sci. Rep.* 2013, **3**, 1836.

(48) Y. Hu, H. Zhang, P. Wu, H. Zhang, B. Zhou and C. Cai, *Phys. Chem. Chem. Phys.* 2011, **13**, 4083.

(49) J. Zhang, H. Yang, J. Fang and S. Zou Nano Lett. 2010, **10**, 638.

(50) C. M. Sanchez-Sanchez, J. Solla-Gullon, F. J. Vidal-Iglesias, A. Aldaz, V. Montiel, and E. Herrero J. Am. Chem. Soc. 2010, **132**, 5622.

(51) N. M. Markovic, H. A. Gasteiger, P. N. Ross J. Phys. Chem. 1996, **100**, 6715.

(52) B. Han, V. Viswanathan, and H. Pitsch J. Phys. Chem. C 2012, **116**, 6174.

(53) P. E. Blochl, *Phy. Rev. B* 1994, **50**, 17953.

(54) G. Kresse and J. Hafner, *Phy. Rev. B* 1993, **47**, 558.

(55) G. Kresse and J. Hafner, *Phy. Rev. B* 1994, **49**, 14251.

(56) G. Kresse and D. Joubert, *Phy. Rev. B* 1999, **59**, 1758.

(57) J. P. Perdew, J. A. Chevary, S. H. Vosko, K. A. Jackson, M. R. Pederson, D. J. Singh and C. Fiolhais, *Phy. Rev. B* 1992, **46**, 6671.

(58) S. Grimme, J. Antony, S. Ehrlich and S.Krieg, *J. Chem. Phys.* 2010, **132**, 154104.

(59) S. Baroni, P, Giannozzi and A.Testa, *Phys. Rev. Lett.* 1987, **58**, 1861.

(60) G. Henkelman and H. Jonsson, *J. Chem. Phys.* 2000, **113**, 9978.

(61) C. Kittel, *Introduction to Solid State Physics,* 8th edition; Hoboken, NJ: John Wiley & Sons: Inc, **2005**.

(62) S. A. Nose, *J. Chem. Phys.* 1984, **81**, 511-519.

(63) Z. Duan and G.Wang, *Phys. Chem. Chem. Phys.* 2011, **13**, 20178.

Published on 09 June 2016. Downloaded by University of Cambridge on 12/06/2016 09:27:53.

Journal of Materials Chemistry A Accepted Manuscript

View Article Online
DOI: 10.1039/C6TA03245A

(64) K. Li, Y. Li, Y. Wang, F. He, M. Jiao, H. Tang and Z. Wu, *J. Mater. Chem. A* 2015, **3**, 11444.

(65) Y. Sha, T. H. Yu, Y. Liu, B. V. Merinov and W. A. Goddard III, *J. Phys. Chem. Lett*. 2010, **1**, 856.

(66) J. A. Keith, G. Jerkiewicz and T. Jacob, *ChemPhysChem* 2010, **11**, 2779.

(67) C. Puglia, A. Nilsson, B. Hernniis, O. Karis, P. Bennich and N. Martensson, *Sur. Sci.* 1995, **342**, 119.

(68) P. D. Nolan, B. R. Lutz, P. L. Tanaka, J. E. Davis and C. B. Mullins, *Phys. Rev. Lett*. 1998, **81**, 3179.

(69) D. H. Parker, M. E. Bartram and B. E. Koel, *Sur. Sci.* 1989, **217**, 489.

(70) H. Steininger and S.; Lehwald and H. Ibach, *Sur. Sci.* 1982, **123**, 1.

(71) B. B. Xiao, Y. F. Zhu, X. Y. Lang, Z. Wen and Q.Jiang, *Sci. Rep.* 2014, **4**, 5205.

(72) J. Yue, Z. Du and M. Shao, *J. Phys. Chem. Lett*. 2015, **6**, 3346.

(73) Y. Y. Yeo, L.Vattuone and D. A King, *J. Chem. Phys.* 1997, **106,** 392.

(74) E. M. Karp, C. T. Campbell, F. Studt, F. Abild-Pedersen and J. K. Norskov, *J. Phys. Chem. C* 2012, **116**, 25772.

(75) P. A. Thiel and T. E. Madey, *Sur. Sci.* 1987, **7**, 211.

(76) G. B. Fisher and J. L. Gland, *Sur. Sci.* 1980, **94**, 446.

(77) Y. Sha, T. H.; Yu, B. V. Merinov, P. Shirvanian and W. A. Goddard, *J. Phys. Chem. Lett*. 2011, **2**, 572.

(78) C. A. Farberow, A. Godinez-Garcia, G. W. Peng, J. F. Perez-Robles, O. Solorza-Feria and M. Mavrikakis, *ACS Catal.* 2013, **3**, 1622.

(79) R. F. W. Bader, Atoms in Molecules: A Quantum Theory; Oxford University Press: USA, **1994.**

(80) G. Henkelman, A. Arnaldsson and H. Jonsson, *Comput. Mater. Sci.* 2006, **36**, 354.

Published on 09 June 2016. Downloaded by University of Cambridge on 12/06/2016 09:27:53.

Journal of Materials Chemistry A Accepted Manuscript

View Article Online
DOI: 10.1039/C6TA03245A

(81) E. Sanville, S. D. Kenny, R. Smith, G. Henkelman, *J. Comput. Chem.* 2007, **28**, 899.

(82) W. Tang, E. Sanville and G. A. Henkelman, *J. Phys.: Condens. Matter.* 2009, **21**, 084204.

(83) P. Strasser, S. Koh, T. Anniyev, J. Greeley, K. More, C. Yu, Z. Liu, S. Kaya, D. Nordlund and H. Ogasawara, M. F. Toney and A. Nilsson, *Nat. Chem.* 2010, **2**, 454.

(84) S. Kattel and G. Wang, *J. Chem. Phys.* 2014, **141**, 124713.

(85) A. Mahata, I. Choudhuri and B. Pathak, *Nanoscale* 2015, **7**, 13438.

(86) V. Mehta and J. S. Cooper, *J. Power Sources* 2003**, 114**, 32.

Published on 09 June 2016. Downloaded by University of Cambridge on 12/06/2016 09:27:53.

Journal of Materials Chemistry A Accepted Manuscript

Table of Content

View Article Online
DOI: 10.1039/C6TA03245A

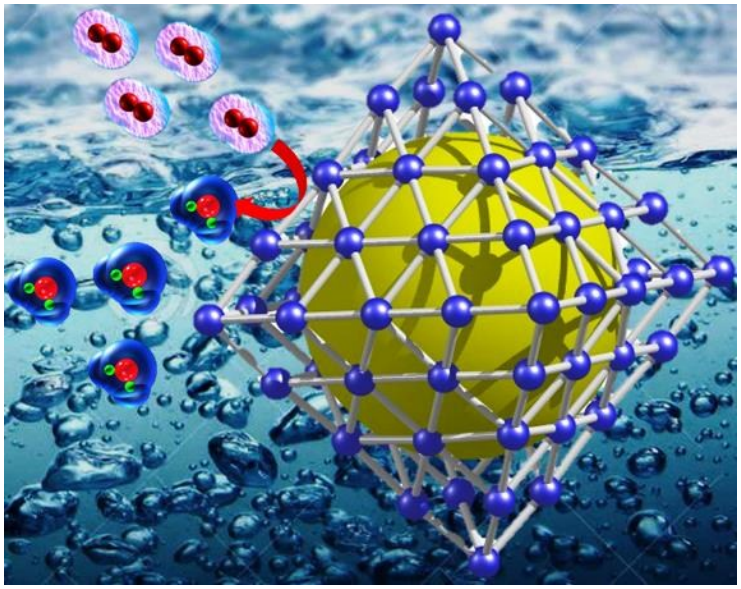

Published on 09 June 2016. Downloaded by University of Cambridge on 12/06/2016 09:27:53.

Journal of Materials Chemistry A Accepted Manuscript